

---

---

# Thymidine Metabolism as a Confounding Factor for 3'-Deoxy-3'-<sup>18</sup>F-Fluorothymidine Uptake After Therapy in a Colorectal Cancer Model

Sonja Schelhaas<sup>1</sup>, Lydia Wachsmuth<sup>2</sup>, Sven Hermann<sup>1</sup>, Natascha Rieder<sup>3</sup>, Astrid Heller<sup>3</sup>, Kathrin Heinzmann<sup>4</sup>, Davina J. Honess<sup>5</sup>, Donna-Michelle Smith<sup>5</sup>, Inga B. Fricke<sup>1</sup>, Nathalie Just<sup>2</sup>, Sabrina Doblas<sup>6</sup>, Ralph Sinkus<sup>7</sup>, Christian Döring<sup>1</sup>, Klaus P. Schäfers<sup>1</sup>, John R. Griffiths<sup>5</sup>, Cornelius Faber<sup>2</sup>, Richard Schneider<sup>8</sup>, Eric O. Aboagye\*<sup>4</sup>, and Andreas H. Jacobs\*<sup>1,9</sup>

<sup>1</sup>European Institute for Molecular Imaging, Westfälische Wilhelms-Universität Münster, Münster, Germany; <sup>2</sup>Department of Clinical Radiology, University Hospital of Münster, Münster, Germany; <sup>3</sup>Pathology and Tissue Analytics, Roche Pharma Research and Early Development, Roche Innovation Center, Munich, Germany; <sup>4</sup>Comprehensive Cancer Imaging Centre, Imperial College London, London, United Kingdom; <sup>5</sup>Cancer Research U.K. Cambridge Institute, Cambridge, United Kingdom; <sup>6</sup>Laboratory of Imaging Biomarkers, UMR 1149-CRI, INSERM, Paris Diderot University, Paris, France; <sup>7</sup>Imaging Sciences and Biomedical Engineering Division, Kings College, London, United Kingdom; <sup>8</sup>Merck KGaA, Darmstadt, Germany; and <sup>9</sup>Department of Geriatric Medicine, Johanniter Hospital, Bonn, Germany

---

Noninvasive monitoring of tumor therapy response helps in developing personalized treatment strategies. Here, we performed sequential PET and diffusion-weighted MRI to evaluate changes induced by a FOLFOX-like combination chemotherapy in colorectal cancer xenografts, to identify the cellular and molecular determinants of these imaging biomarkers. **Methods:** Tumor-bearing CD1 nude mice, engrafted with FOLFOX-sensitive Colo205 colorectal cancer xenografts, were treated with FOLFOX (5-fluorouracil, leucovorin, and oxaliplatin) weekly. On days 1, 2, 6, 9, and 13 of therapy, tumors were assessed by in vivo imaging and ex vivo analyses. In addition, HCT116 xenografts, which did not respond to the FOLFOX treatment, were imaged on day 1 of therapy. **Results:** In Colo205 xenografts, FOLFOX induced a profound increase in uptake of the proliferation PET tracer 3'-deoxy-3'-<sup>18</sup>F-fluorothymidine (<sup>18</sup>F-FLT) accompanied by increases in markers for proliferation (Ki-67, thymidine kinase 1) and for activated DNA damage response (γH2AX), whereas the effect on cell death was minimal. Because tracer uptake was unaltered in the HCT116 model, these changes appear to be specific for tumor response. **Conclusion:** We demonstrated that <sup>18</sup>F-FLT PET can noninvasively monitor cancer treatment-induced molecular alterations, including thymidine metabolism and DNA damage response. The cellular or imaging changes may not, however, be directly related to therapy response as assessed by volumetric measurements.

**Key Words:** <sup>18</sup>F-FLT PET; DW-MRI; combination cancer therapy; small-animal imaging

**J Nucl Med 2018; 59:1063–1069**

DOI: 10.2967/jnumed.117.206250

**C**olorectal cancer (CRC) is the third most common cancer and the fourth most common cause of cancer-related deaths worldwide (1). FOLFOX, the combination of oxaliplatin, 5-fluorouracil (5-FU), and leucovorin (folinic acid), is a frequently used therapy for CRC. The active metabolites of 5-FU disrupt RNA synthesis and inhibit thymidylate synthase (TS), an enzyme important for DNA synthesis. This TS inhibitory activity can be enhanced by leucovorin (2). The combination of these 2 agents has been shown to be superior to therapy with 5-FU alone in patients with advanced CRC (3). Oxaliplatin is a third-generation platinum analog, inducing DNA intra- and interstrand crosslinks, which ultimately result in cell death (4). The addition of oxaliplatin to the combination of 5-FU and leucovorin is beneficial to outcome—for instance, in the adjuvant (5) setting.

Molecular imaging can aid in early and noninvasive identification of patients not responding to therapy, allowing an early change in treatment approach. This not only reduces unnecessary side effects for the patient but also allows for early definition of effective treatment. PET with <sup>18</sup>F-FDG is routinely used in the clinic for tumor therapy follow-up. A drawback of <sup>18</sup>F-FDG is its accumulation in inflammatory lesions (6). The proliferation tracer 3'-deoxy-3'-<sup>18</sup>F-fluorothymidine (<sup>18</sup>F-FLT), a thymidine analog, performs better than <sup>18</sup>F-FDG with regard to selectivity and has already been successfully used for monitoring tumor response to therapy in a range of pre-clinical and clinical studies (7,8). <sup>18</sup>F-FLT is phosphorylated by thymidine kinase 1 (TK1) and retained within proliferative cells. Therefore, uptake of <sup>18</sup>F-FLT reflects the thymidine salvage pathway (9), an alternative thymidine-to-DNA pathway to the de novo pathway, with the key enzyme TS. Thymidine phosphorylase (TP) affects <sup>18</sup>F-FLT uptake by degrading thymidine, whereas <sup>18</sup>F-FLT is resistant to the activity of this enzyme (10). It is well recognized that thymidine competes with <sup>18</sup>F-FLT for cellular retention (11) and that this competition can be modified by TP (12,13). Moreover, TP activity plays a role in tumor angiogenesis, induces metastasis, and protects cancer cells against apoptosis (14).

Another method for noninvasive monitoring of response to therapy is diffusion-weighted MRI. Tumor cell killing as a consequence of

---

Received Nov. 30, 2017; revision accepted Jan. 22, 2018.

For correspondence or reprints contact: Andreas H. Jacobs, European Institute for Molecular Imaging, Waldeyerstrasse 15, 48149 Münster, Germany.

E-mail: ahjacobs@uni-muenster.de

\*Contributed equally to this work.

Published online Feb. 23, 2018.

COPYRIGHT © 2018 by the Society of Nuclear Medicine and Molecular Imaging.

successful therapy results in increased intercellular space and hence enhanced water diffusion, measured as an increase in the apparent diffusion coefficient (ADC) (15).

Here, we used CRC models treated with a FOLFOX-like combination therapy, which we refer to as FOLFOX. We evaluated changes in uptake of the radiotracers  $^{18}\text{F}$ -FLT and  $^{18}\text{F}$ -FDG, as well as in ADC measured by diffusion-weighted MRI, and analyzed associated alterations within the tumors on a cellular level. This will allow a better understanding of tumor biology and factors affecting imaging biomarkers, paving the way for improved cancer therapy in the clinical setting.

## MATERIALS AND METHODS

### Animal Model

Colo205 and HCT116 cells were cultivated in Dulbecco modified Eagle medium and RPMI medium, respectively, supplemented with 10% fetal calf serum, penicillin (100 U/mL), and streptomycin (100  $\mu\text{g}/\text{mL}$ ). Animal procedures were performed in accordance with the German Laws for Animal Protection and were approved by the animal care committee of the local government (North Rhine-Westphalia State Agency for Nature, Environment, and Consumer Protection). Female CD1 nude mice 6–8 wk old (Charles River Laboratories) received a subcutaneous injection of  $5 \times 10^6$  Colo205 or  $2 \times 10^6$  HCT116 cells into the shoulder region. Two tumors were inoculated per animal, and growth was followed by digital caliper measurements (volume =  $\frac{1}{2}$  (length  $\times$  width $^2$ )).

Animals were assigned randomly to groups. FOLFOX therapy was applied weekly. The treatment was started with intraperitoneal oxaliplatin (8 mg/kg) followed by retrobulbar leucovorin 1.5 h later (90 mg/kg) and 2 intraperitoneal doses of 5-FU (30 mg/kg at 2 h and 6 h after treatment initiation). All agents were obtained from the pharmacy of the University Hospital of Münster. Control animals were injected with the respective solvents at the same time points. 5-FU therapy consisted of 2 doses of 5-FU only (30 mg/kg each, given 4 h apart). The experimental schedule is presented in Supplemental Table 1 (supplemental materials are available at <http://jnm.snmjournals.org>).

### $^{18}\text{F}$ -FLT and $^{18}\text{F}$ -FDG PET Imaging and Analysis

$^{18}\text{F}$ -FLT was synthesized as reported previously (16). A 10-MBq dose of tracer was injected into isoflurane-anesthetized mice. Imaging was performed 70–90 min afterward using a quadHIDAC PET device (Oxford Positron Systems). A multimodal bed was used to transfer the animal to a Bruker MR tomograph for diffusion-weighted MRI during the tracer uptake period or to a CT scanner (Inveon; Siemens Medical Solutions) after completion of the PET scan.

$^{18}\text{F}$ -FDG was synthesized according to a previously published report (17). A 10-MBq dose of tracer was injected into anaesthetized nonfasting mice.  $^{18}\text{F}$ -FDG PET images were acquired 60–75 min after tracer application using a small-animal PET/MRI device (nanoScan PET/MRI; Mediso Medical Imaging Systems), and the integrated 1-T MR tomograph was used to acquire respective morphologic information (T1-weighted imaging; repetition/echo time, 17.1/3.8 ms; field of view, 100 mm; slice thickness, 0.5 mm; 400 matrix).

Volumes of interest were drawn manually on anatomic images and transferred to the respective PET images using MEDgical, an in-house-developed software for multimodal data analysis. The whole tumor was defined by the volume of interest, and tracer uptake was expressed as  $\text{SUV}_{\text{max}}$ . The data confirmed that the results and conclusions were not dependent on the method of analysis.

### Diffusion-Weighted MRI

A Bruker Biospec 9.4-T tomograph was used to obtain data on water diffusion. T2-weighted images were acquired first (2-dimensional rapid

acquisition with relaxation enhancement; repetition/echo time, 3,600/40 ms; rapid-acquisition-with-relaxation-enhancement factor, 8; field of view, 35 mm; 256 matrix; slice thickness, 1 mm; 4 slices per tumor at the largest tumor diameter), followed by diffusion-weighted images (echo planar imaging–diffusion tensor imaging; repetition/echo time, 1,000/19 ms; 12 segments; 7 b-values from 0 to 700  $\text{s}/\text{mm}^2$ ; 128 matrix; number of excitations, 6; respiration-triggered). ADC values were analyzed with the software Beaugui developed at INSERM. ADC maps were calculated on a pixel-by-pixel basis using this software based on ROOT (version 5.34.01; CERN). The ADC was calculated by fitting the normalized signal intensity to a classic monoexponential model (cutoff  $> 150 \text{ s}/\text{mm}^2$ ), using a nonlinear least-squares approach with a Levenberg–Marquardt algorithm. Tumor regions of interest were defined manually on the  $b = 0$  images and then copied onto the ADC maps to determine  $\text{ADC}_{\text{mean}}$ .

### Immunohistochemistry

Formalin-fixed tumor tissue was embedded in paraffin, and 2.5- $\mu\text{m}$  sections were analyzed. Hematoxylin and eosin staining was performed on an automated Symphony system (Ventana Medical Systems) using reagents from Ventana Medical Systems. Immunohistochemistry for Ki-67 was performed on a Discovery XT automated stainer (Ventana Medical Systems) using Ventana Medical Systems reagents. After mild treatment with tris-based cell conditioning 1, we applied Confirm anti-Ki-67 (clone 30-9) rabbit monoclonal antibody (ready-to-use dispenser, catalog no. 790-4286; Ventana Medical Systems). Positive immunoreactivity was detected with an OmniMap detection system (Ventana Medical Systems).

The slides were scanned at  $\times 20$  using an iScan HT device (Ventana Medical Systems), and the digital images were analyzed using automated analysis algorithms from the Roche digital pathology platform Iris. The whole process was supervised by an expert pathologist, who controlled the quality of the algorithm performance. Annotation of tumor area on the hematoxylin and eosin slide by the pathologist was followed by automated segmentation into tumor and necrosis areas. Image registration of the hematoxylin and eosin slide and the consecutive Ki-67 slide was performed, and viable tumor area was transferred onto the Ki-67 slide. Automatic classification into Ki-67–positive tumor nuclei and Ki-67–negative nuclei resulted in reporting of Ki-67–positive and –negative tumor nuclei and analyzed area, cellularity (tumor nuclei per area), and percentage Ki-67 positivity of tumor nuclei. Heat maps of the density of Ki-67–positive nuclei are shown for visualization.

For all further immunohistochemistry, 5- $\mu\text{m}$  sections were incubated overnight at 4°C with the primary antibody (1:200 TK1 [EPR3193; Abcam]; 1:100 active caspase-3 [CPP32; BD Pharmingen]; or 1:100  $\gamma\text{H2AX}$  [catalog no. 9718; Cell Signaling Technology]). Cell death was detected by a commercially available kit (in situ TUNEL kit assay; Roche). Images were acquired using an Eclipse 90i microscope (Nikon) and the NIS-Elements software package (Nikon). Positively stained areas in regions of viable tumor tissue were determined on 5–8 images ( $\times 20$ ) per tumor with the software ImageJ (National Institutes of Health).

### Thymidine Analysis

Thymidine in tumors and plasma was quantified as described previously (18).

### Western Blot Analysis

Tumor tissue was lysed in radioimmunoprecipitation assay buffer with a Precellys 24 homogenizer/lysing kit (1.4 mm ceramic beads; Bertin Instruments). Polyacrylamide gel electrophoresis was performed with 4%–15% Mini-Protean TGX Precast Gels (BioRad), 15-well. After transfer to a Trans-Blot Turbo Midi Nitrocellulose membrane (BioRad), proteins were probed overnight at 4°C with primary antibodies against TK1 (1:5,000; ab76495 [Abcam]), TS (1:1,000; 3766S [Cell

Signaling Technologies)], TP (1:2,000; 12383-1AP [Acris]), or actin (1:10,000; ab6276 [Abcam]). Goat anti-rabbit (1:10,000; sc-2004 [Santa Cruz]) and goat anti-mouse (1:10,000; sc-2005 [Santa Cruz]) were used as secondary antibodies. Signals were then revealed with Amersham ECL Western blotting detection reagents and Amersham Hyperfilm ECL (both GE Healthcare). ImageJ was used for quantification via densitometry, and protein levels are expressed relative to an actin loading control.

### Statistics

Results are expressed as box plots showing the median and the 25th and 75th percentiles. Error bars depict ranges. Mean and SD were plotted for correlation analyses. Significance was calculated with SigmaPlot software (version 13; Systat Software Inc). Because not all data were normally distributed, we used the Mann–Whitney rank sum test to compare groups. Correlations were determined with the Spearman correlation coefficient. All numeric data and sample sizes are presented in the supplemental materials.

## RESULTS

### Molecular Imaging of Treatment Response in Colo205 Xenografts

We established a FOLFOX treatment regimen that closely resembles the therapy schedule used in the clinical situation. When given weekly, the therapy inhibited the growth of Colo205 xenografts (Fig. 1A; Supplemental Table 2), implying that these tumors are sensitive to FOLFOX.

$^{18}\text{F}$ -FLT PET imaging revealed a remarkable increase of tracer uptake in FOLFOX-treated Colo205 xenografts at all time points investigated (Figs. 1B and C; Supplemental Table 3). The largest increase was 1 d after therapy (9.2-fold relative to baseline and 10.1-fold relative to control). At the end of a treatment cycle (days 6 and 13), tracer uptake approached baseline levels but was still significantly enhanced. A potential cause of increased  $^{18}\text{F}$ -FLT could be the TS inhibitory activity of 5-FU. Therefore, we analyzed  $^{18}\text{F}$ -FLT uptake in tumors treated with 5-FU on the first day of therapy, when the strongest induction of  $^{18}\text{F}$ -FLT accumulation could be observed after combination therapy. 5-FU caused a remarkable increase in  $^{18}\text{F}$ -FLT  $\text{SUV}_{\text{max}}$  (control,  $1.6 \pm 0.4$ ; 5-FU,  $11.6 \pm 2.5$  [ $P < 0.01$ , 7.1-fold relative to control]) (Fig. 1C). However, the FOLFOX combination resulted in an even stronger increase ( $16.5 \pm 2.0$ ;  $P < 0.01$  relative to 5-FU), indicating that 5-FU alone is not responsible for the total extent of  $^{18}\text{F}$ -FLT uptake after FOLFOX therapy. Also other modes of  $^{18}\text{F}$ -FLT PET quantification were applied (Supplemental Table 3), confirming that the results and conclusions were not dependent on the method of analysis.

We also performed longitudinal diffusion-weighted MRI studies on FOLFOX-treated tumors (Fig. 1D; Supplemental Table 4). The resulting ADC maps showed a variable and heterogeneous distribution of water diffusion (Supplemental Fig. 1). Tumors tended to have lower ADC values over time, irrespective of treatment. Relative to baseline, the  $\text{ADC}_{\text{mean}}$  of FOLFOX-treated tumors was significantly decreased on days 2, 6, 9, and 13, and the  $\text{ADC}_{\text{mean}}$  of control-treated tumors was significantly decreased on day 9. Tumors of FOLFOX-treated mice tended to have higher ADC values than tumors of control-treated animals, an effect that was significant on day 9. 5-FU treatment alone did not result in changes of water diffusion on day 1.

### Ex Vivo Analyses of FOLFOX-Treated Colo205 Xenografts

Immunohistochemistry showed an increase of Ki-67 and TK1 staining in the FOLFOX-treated tumors (Fig. 2; Supplemental Table 5), implying an increase of cellular proliferation. Elevated TK1

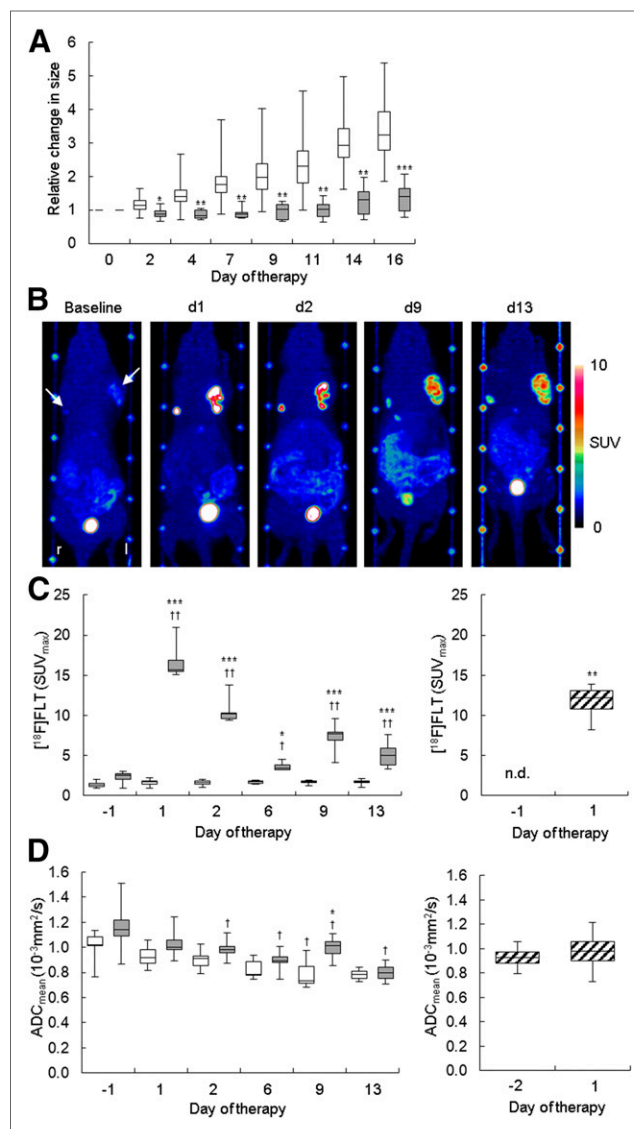


**FIGURE 1.** In Colo205 xenografts, FOLFOX therapy resulted in tumor growth arrest, increase in  $^{18}\text{F}$ -FLT uptake, and no increase in  $\text{ADC}_{\text{mean}}$ . (A) Caliper measurements revealed FOLFOX to have a growth inhibitory effect that was already significant on day 2 of therapy. (B) Maximum-intensity projections of a representative FOLFOX-treated mouse show that tumor  $^{18}\text{F}$ -FLT uptake was remarkably enhanced after therapy. Imaging on day 6 was not performed on the mouse presented here. Images also show fiducial markers used for coregistration with MR images. Arrows point to 2 tumors. (C) Quantification of tumor  $^{18}\text{F}$ -FLT uptake revealed remarkable increase of  $\text{SUV}_{\text{max}}$  relative to baseline after FOLFOX. (D) Significant reductions in  $\text{ADC}_{\text{mean}}$  relative to baseline could be observed during growth of FOLFOX- and control-treated tumors. White bars = control; gray bars = FOLFOX; striped bars = 5-FU. \* $P < 0.05$ , \*\* $P < 0.01$ , and \*\*\* $P < 0.001$  relative to control. † $P < 0.05$  and †† $P < 0.01$  relative to baseline.

staining was also noted on day 1 when mice were treated with 5-FU alone. No statistically significant association of  $^{18}\text{F}$ -FLT with Ki-67 immunohistochemistry could be detected. However, a correlation with TK1 ( $\rho = 0.893$ ,  $P < 0.001$ ) was observed.

Western blot analysis confirmed an increase in TK1 expression after FOLFOX therapy and also indicated upregulation of the other thymidine metabolism proteins, TS and TP (Supplemental Fig. 2;

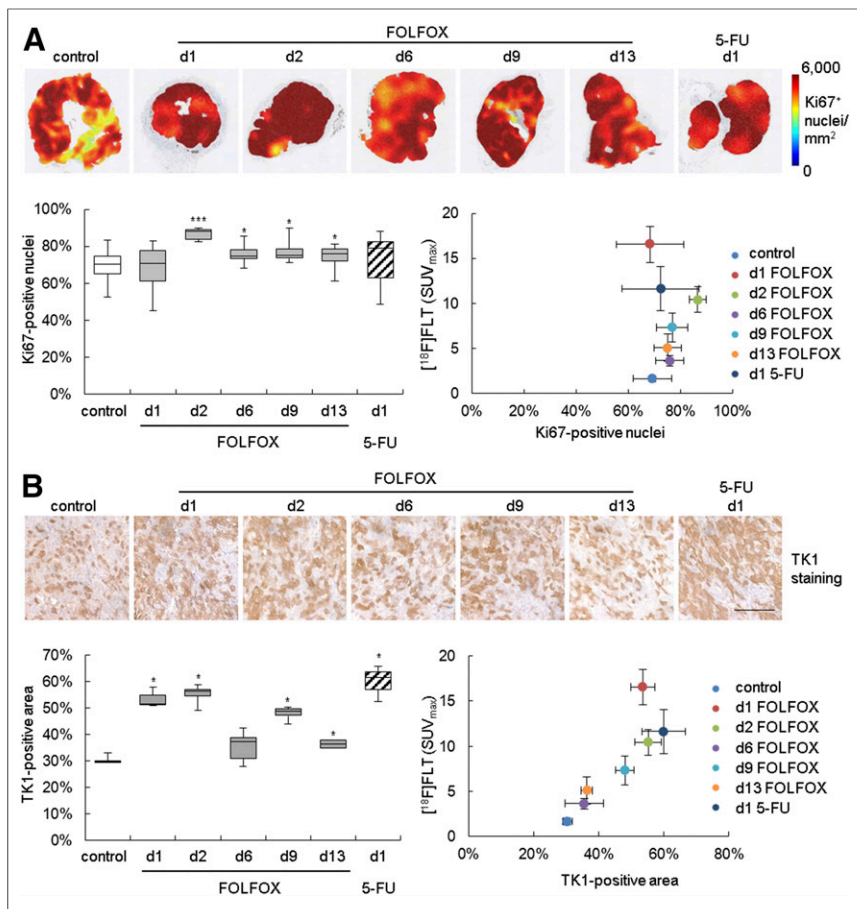


**FIGURE 2.** In Colo205-bearing mice, FOLFOX therapy resulted in increase of histologic proliferation markers. (A) Heat maps depicting density of Ki-67–positive nuclei of representative tumors are shown in upper panel. Percentage positive nuclei was quantified and related to <sup>18</sup>F-FLT uptake. (B) TK1 staining was quantified as positively stained area. Scale bar = 100  $\mu$ m. d = day; white bars = control; gray bars = FOLFOX; striped bars = 5-FU. \* $P < 0.05$  and \*\*\* $P < 0.001$  relative to control.

Supplemental Table 6). This finding prompted us to analyze tumor and plasma thymidine levels, which were decreased at later time points in FOLFOX-treated animals (Fig. 3; Supplemental Table 7).

Immunohistochemical analysis of cleaved caspase-3 and a TUNEL assay revealed an increased level of cell death only after the second treatment (days 9 and 13) (Fig. 4; Supplemental Table 8). Other histologic markers of cell death were not altered (Supplemental Fig. 3).

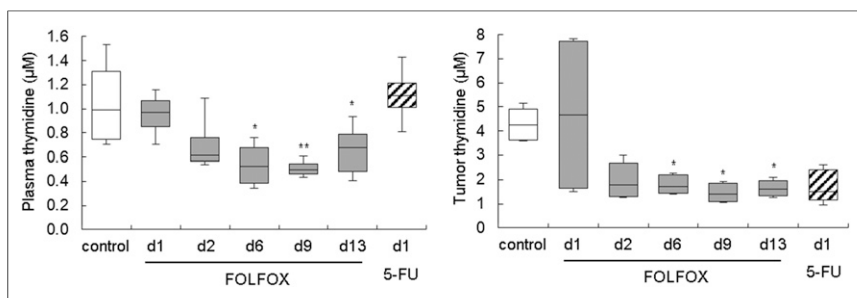


**FIGURE 3.** Thymidine levels were decreased in FOLFOX-treated Colo205 tumors, as measured by liquid chromatography tandem mass spectrometry. d = day; white bars = control; gray bars = FOLFOX; striped bars = 5-FU. \* $P < 0.05$  and \*\* $P < 0.01$  relative to control.

Many therapeutic agents induce double-strand breaks in DNA, which activate cellular DNA damage response (DDR) mechanisms. A key step of DDR is phosphorylation of the histone variant H2AX, producing  $\gamma$ H2AX, which is required for assembly of DNA repair proteins (19). Analysis of  $\gamma$ H2AX revealed prolonged activation of DDR after FOLFOX treatment in Colo205 xenografts and 1 d after 5-FU treatment (Fig. 5; Supplemental Table 9). <sup>18</sup>F-FLT uptake correlated with  $\gamma$ H2AX staining ( $\rho = 0.964$ ,  $P < 0.001$ ).

### <sup>18</sup>F-FLT PET Imaging of Nonresponsive HCT116 Xenografts

HCT116 xenografts appear to be non-responsive to FOLFOX, as their growth was not impaired even after 3 cycles of therapy (Fig. 6A; Supplemental Table 10). We analyzed changes of <sup>18</sup>F-FLT on day 1 after therapy, as the <sup>18</sup>F-FLT increase was most pronounced at this time point. No alteration of <sup>18</sup>F-FLT was observed in HCT116 tumors (Fig. 6B; Supplemental Table 11).

### DISCUSSION

Longitudinal molecular imaging in conjunction with ex vivo molecular analyses was performed to investigate alterations induced by a FOLFOX-like combination therapy in CRC models in a clinically translatable approach. FOLFOX induced a substantial increase in <sup>18</sup>F-FLT uptake, corresponding to sustained increases in DDR and proliferation markers. In contrast, <sup>18</sup>F-FLT was unaltered in nonresponding HCT116 xenografts, implying that the observed increase is predictive for therapy response. Prolonged activation of DDR is most likely responsible for the absence of any major changes in tumor cell death, which were reflected by unaltered water diffusivity, as assessed by diffusion-weighted MRI. We speculate that the observed alterations are based on this tumor possessing a DNA repair–proficient metabolic phenotype, with delayed onset of cell death involving enhanced requirements for nucleosides via the salvage pathway.

Because <sup>18</sup>F-FLT PET is thought to report tumor proliferation, and diffusion-weighted MRI is sensitive to the increase in ADC as a consequence of cell death, the 2 methods are complementary, particularly for monitoring the response of tumors to chemotherapy. This allows a comprehensive assessment of the biologic processes engaged, potentially improving care of cancer patients, especially when the 2 imaging modalities are combined.

The increase in <sup>18</sup>F-FLT uptake in FOLFOX-treated xenografts was remarkable. Because growth was arrested in the treated

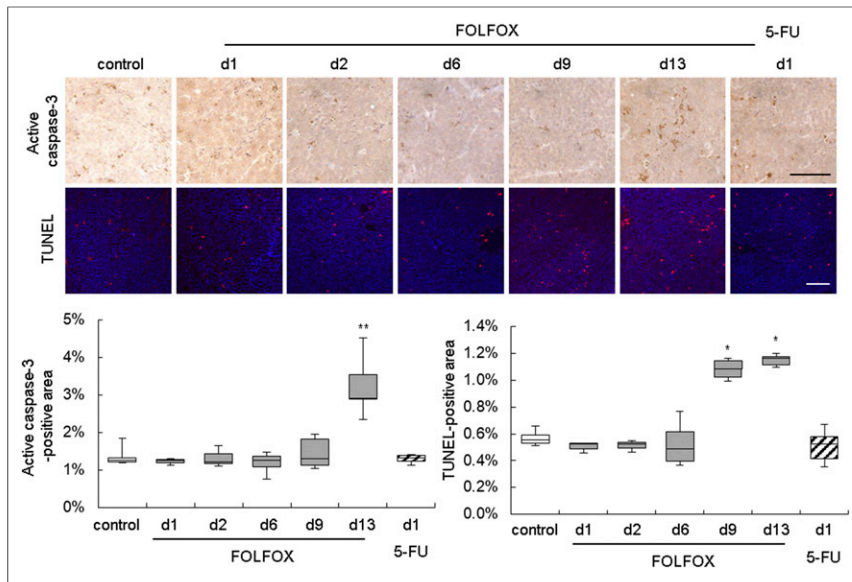


**FIGURE 4.** Immunohistochemistry of activated caspase-3 and TUNEL assay of Colo205 tumors implied increase in cell death after second FOLFOX treatment. Scale bar = 100  $\mu$ m. d = day; white bars = control; gray bars = FOLFOX; striped bars = 5-FU. \* $P$  < 0.05 and \*\* $P$  < 0.01 relative to control.

tumors, one would expect a decrease in uptake of this proliferation tracer rather than an increase. In addition, we observed a significant increase in Ki-67 immunohistochemical staining. This increase contradicts the normal expectation of reduced proliferation in tumors whose growth is arrested but is in line with a clinical study that observed increased Ki-67 expression in CRC liver metastases after FOLFOX therapy (20). The authors of that study concluded that the increase could have resulted from increased proliferation and migration induced by an autocrine mechanism that might be used by metastatic cells escaping FOLFOX-induced cell death. Possibly, the Ki-67 signal in our tumor model arose from an increase in the number of proliferating tumor cells relative to nonproliferating tumor cells. Tumor volume measurements showed that even though tumor volumes were still significantly reduced relative to controls in the third week of treatment, the tumors tended to grow again, implying

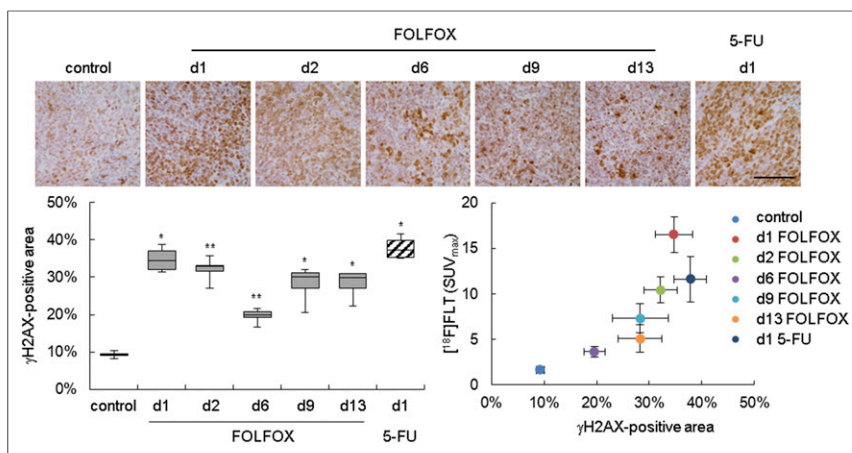


**FIGURE 5.** DDR was activated after FOLFOX therapy as determined by immunohistochemistry of  $\gamma$ H2AX. Positively stained area was quantified and related to  $^{18}$ F-FLT uptake. Scale bar = 100  $\mu$ m. d = day; white bars = control; gray bars = FOLFOX; striped bars = 5-FU. \* $P$  < 0.05 and \*\* $P$  < 0.01 relative to control.

that there are indeed proliferative tumor cells present in the FOLFOX-treated xenografts.

Western blot analysis implied that TP, TS, and TK1 were also upregulated, even though they are involved in opposing thymidine pathways. These results were not statistically significant using nonparametric tests, likely because of the low sample number. However, it is likely that they are of biologic relevance. TS might be upregulated as a mechanism of resistance to 5-FU therapy (21), and oxaliplatin has been shown to increase expression of TP (22). Increased TK1 expression was in line with respective TK1 immunohistochemistry. It has already been reported that inhibition of TS by 5-FU can induce upregulation of TK1, resulting in increased accumulation of  $^{18}$ F-FLT (23). In our study, TK1 expression paralleled  $^{18}$ F-FLT uptake. At the end of a treatment cycle, both approached the levels of controls, implying that tumor biology recedes to baseline levels. This recession could be caused by the limited plasma half-lives of the therapeutic agents used.

Thymidine within tumors and plasma was decreased on days 6, 9, and 13, as could be provoked by the catalytic activity of TP (10). Furthermore, TS-inhibiting agents such as 5-FU can induce the thymidine salvage pathway, resulting in enhanced use of thymidine (24). In our model, diminished levels of thymidine might also contribute to the increased uptake of  $^{18}$ F-FLT in tumors, because thymidine and  $^{18}$ F-FLT compete for cellular uptake and retention (11).

Most of the observed changes (upregulation of thymidine pathway enzymes and  $^{18}$ F-FLT) can probably be attributed to the action of 5-FU. However, we demonstrated that equivalent doses of 5-FU alone lead to a less pronounced increase in  $^{18}$ F-FLT than the increase provoked by FOLFOX, suggesting that in our therapy model TS inhibition is amplified relative to that caused by 5-FU alone. Leucovorin stabilizes the complex of 5-FU with TS. Furthermore, it is likely that an oxaliplatin-induced increase in TP expression improves 5-FU activity, because TP converts 5-FU to one of its active metabolites, 5-fluoro-2'-deoxyuridine (14). It would be interesting to investigate whether the differences in TS inhibition and  $^{18}$ F-FLT uptake are related to differences in tumor growth inhibition.

The increase in  $^{18}$ F-FLT uptake in the FOLFOX-responsive Colo205 model appears to be predictive for therapy response, as  $^{18}$ F-FLT was unchanged in the nonresponsive HCT116 xenografts. Consequently, an increase in  $^{18}$ F-FLT accumulation is possibly a prognostic marker for this treatment approach. This hypothesis is strengthened by a clinical feasibility study by Kenny et al. measuring  $^{18}$ F-FLT uptake 1 h after treatment with the 5-FU prodrug capecitabine (25). This study showed that in breast cancer patients who progressed on therapy, the

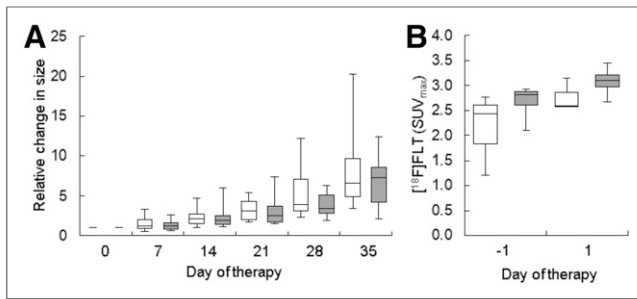


**FIGURE 6.** FOLFOX therapy in HCT116 xenografts affected neither tumor growth nor <sup>18</sup>F-FLT uptake. (A) Tumor volumes were determined by caliper measurements. Therapy was applied weekly. (B) <sup>18</sup>F-FLT accumulation was not significantly altered. White bars = control; gray bars = FOLFOX.

tracer uptake parameters did not change, whereas they were increased in responders. In contrast, Hong et al. observed an increase in <sup>18</sup>F-FLT uptake on day 2 after initiation of FOLFOX treatment in CRC patients—an increase that was more pronounced in nonresponders than in responders (26). Some clinical and preclinical studies have shown that nontherapeutic doses of TS-inhibiting agents can also increase <sup>18</sup>F-FLT (27–29), indicating that this change is not predictive of tumor therapy response to these drugs. Thus, further investigations are needed to assess the role of <sup>18</sup>F-FLT in predicting response to TS-inhibiting therapy.

In Colo205 xenografts, we also performed PET imaging with the clinically established metabolism tracer <sup>18</sup>F-FDG (Supplemental Fig. 4; Supplemental Table 12). <sup>18</sup>F-FDG uptake was not consistently altered and therefore did not reflect FOLFOX effects. Moreover, because <sup>18</sup>F-FDG accumulates in inflammatory lesions, the unchanged <sup>18</sup>F-FDG also implies that the increase in <sup>18</sup>F-FLT observed in this study was not caused by inflammatory cells.

In our study, tumor cell death was only slightly increased within the second FOLFOX treatment cycle, as measured by caspase-3 immunohistochemistry and TUNEL. In contrast, other histologic markers of cell death (cellular density, necrotic area) were unaltered. These results provide a plausible explanation for why we did not detect a FOLFOX-induced increase of ADC<sub>mean</sub>. The observed differences in water diffusion occurred at all time points investigated and do not appear to be of physiologic relevance.

Histologic analysis revealed sustained activation of the DDR marker  $\gamma$ H2AX after FOLFOX or 5-FU therapy—an effect that could be caused by oxaliplatin or 5-FU (30,31). 5-FU-induced DDR has been described to occur in S phase (32). Hence, it is likely that the DDR observed here is also linked to this phase, as is in line with sustained TK1 expression, which is S-phase-specific. In our study, elevated  $\gamma$ H2AX was observed at all time points, even though levels approached those of control levels at the end of the first treatment cycle (day 6). Decreasing  $\gamma$ H2AX expression might suggest either successful repair of the DNA damage or lysis of dead cells (33). Because no induction of cell death was observed on day 6 after FOLFOX and immunohistochemical markers of proliferation were increased, it is likely that the DNA damage was successfully repaired. Hence, attempts of the tumor cell to repair DNA double-strand breaks might delay induction of cell death, explaining unchanged ADC<sub>mean</sub>.

Increased amounts of nucleosides are needed during DDR. Consequently, DDR in the treated tumors could potentially contribute to the increased <sup>18</sup>F-FLT uptake observed here.  $\gamma$ H2AX expression

parallels <sup>18</sup>F-FLT uptake, and we found a correlation between <sup>18</sup>F-FLT uptake and  $\gamma$ H2AX expression, supporting our hypothesis of increased nucleoside consumption during DDR.

A limitation of this study is that we did not evaluate tumors treated with single agents, apart from the analysis of a single time point for 5-FU. Such an analysis would help to assess the relative contribution of each agent to the observed changes. However, single agents are rarely used in the clinical setting. Therefore, our data shed light on changes induced by a clinically relevant therapy approach. It would be of interest to assess FOLFOX-induced mechanisms in a broader panel of tumor types including nonresponsive models and clinical tumor specimens.

## CONCLUSION

Factors resulting in an increase of <sup>18</sup>F-FLT uptake can be manifold, including increased cellular proliferation (Ki-67), DNA-salvage-pathway use (TK1), and DDR activity, as well as thymidine levels. These parameters might be modulated by tumor treatment, as demonstrated here for a FOLFOX combination therapy as well as a 5-FU monotherapy. Consequently, in this scenario, changes in <sup>18</sup>F-FLT reflect alterations in these pathways not directly related to tumor therapy response, because in general a reduced proliferation (and <sup>18</sup>F-FLT accumulation) is associated with tumor therapy response.

## DISCLOSURE

The research leading to these results has received support from the Innovative Medicines Initiative Joint Undertaking ([www.imi.europa.eu](http://www.imi.europa.eu)) under grant agreement 115151, resources of which are composed of financial contributions from the European Union's Seventh Framework Program (FP7/2007-2013) and EFPIA companies' in-kind contribution. This work was also supported by the Deutsche Forschungsgemeinschaft (DFG) Cluster of Excellence 'Cells-in-Motion' (EXC1003 - CiM), University of Münster, Germany; the Interdisciplinary Centre for Clinical Research (IZKF, core unit PIX), Münster, Germany; and core funding from Cancer Research U.K. (C2536/A16584). No other potential conflict of interest relevant to this article was reported.

## ACKNOWLEDGMENTS

We acknowledge Saeedeh Amirmohseni, Christine Bätza, Florian Breuer, Stefanie Bouma, Irmgard Hoppe, Sarah Köster, Christa Möllmann, Roman Priebe, and Dirk Reinhardt for excellent technical support.

## REFERENCES

1. Global Burden of Disease Cancer Collaboration. The Global Burden of Cancer 2013. *JAMA Oncol.* 2015;1:505–527.
2. Longley DB, Harkin DP, Johnston PG. 5-fluorouracil: mechanisms of action and clinical strategies. *Nat Rev Cancer.* 2003;3:330–338.
3. Poon MA, O'Connell MJ, Wieand HS, et al. Biochemical modulation of fluorouracil with leucovorin: confirmatory evidence of improved therapeutic efficacy in advanced colorectal cancer. *J Clin Oncol.* 1991;9:1967–1972.
4. Raymond E, Faivre S, Woynarowski JM, Chaney SG. Oxaliplatin: mechanism of action and antineoplastic activity. *Semin Oncol.* 1998;25(2, suppl 5):4–12.
5. André T, Boni C, Mounedji-Boudiaf L, et al. Oxaliplatin, fluorouracil, and leucovorin as adjuvant treatment for colon cancer. *N Engl J Med.* 2004;350:2343–2351.
6. Strauss LG. Fluorine-18 deoxyglucose and false-positive results: a major problem in the diagnostics of oncological patients. *Eur J Nucl Med.* 1996;23:1409–1415.
7. Schelhaas S, Heinzmann K, Bollineni VR, et al. Preclinical applications of 3'-deoxy-3'-<sup>18</sup>F-fluorothymidine in oncology: a systematic review. *Theranostics.* 2017;7:40–50.

8. Bollineni VR, Kramer GM, Jansma EP, Liu Y, Oyen WJG. A systematic review on <sup>18</sup>F-FLT-PET uptake as a measure of treatment response in cancer patients. *Eur J Cancer*. 2016;55:81–97.
9. Shields AF, Grierson JR, Dohmen BM, et al. Imaging proliferation in vivo with [<sup>18</sup>F]-FLT and positron emission tomography. *Nat Med*. 1998;4:1334–1336.
10. Toyohara J, Fujibayashi Y. Trends in nucleoside tracers for PET imaging of cell proliferation. *Nucl Med Biol*. 2003;30:681–685.
11. Zhang CC, Yan Z, Li W, et al. <sup>18</sup>F-FLT-PET imaging does not always “light up” proliferating tumor cells. *Clin Cancer Res*. 2012;18:1303–1312.
12. Schelhaas S, Wachsmuth L, Viel T, et al. Variability of proliferation and diffusion in different lung cancer models as measured by 3'-deoxy-3'-<sup>18</sup>F-fluorothymidine PET and diffusion-weighted MR imaging. *J Nucl Med*. 2014;55:983–988.
13. Schelhaas S, Heinzmann K, Honess DJ, et al. 3'-deoxy-3'-<sup>18</sup>F-fluorothymidine uptake is related to thymidine phosphorylase expression in various experimental tumor models. *Mol Imaging Biol*. 2018;20:194–199.
14. Bronckaers A, Gago F, Balzarini J, Liekens S. The dual role of thymidine phosphorylase in cancer development and chemotherapy. *Med Res Rev*. 2009;29:903–953.
15. Sinkus R, Van Beers BE, Vilgrain V, DeSouza N, Waterton JC. Apparent diffusion coefficient from magnetic resonance imaging as a biomarker in oncology drug development. *Eur J Cancer*. 2012;48:425–431.
16. Viel T, Schelhaas S, Wagner S, et al. Early assessment of the efficacy of temozolomide chemotherapy in experimental glioblastoma using <sup>18</sup>F-FLT-PET imaging. *PLoS One*. 2013;8:e67911.
17. Füchtner F, Steinbach J, Mäding P, Johannsen B. Basic hydrolysis of in the preparation of 2-<sup>18</sup>F-fluoro-2-deoxy-d-glucose. *Appl Radiat Isot*. 1996;47:61–66.
18. Heinzmann K, Honess DJ, Lewis DY, et al. The relationship between endogenous thymidine concentrations and <sup>18</sup>F-FLT uptake in a range of preclinical tumour models. *EJNMMI Res*. 2016;6:63.
19. Podhorecka M, Skladanowski A, Bozko P. H2AX phosphorylation: its role in DNA damage response and cancer therapy. *J Nucleic Acids*. 2010;2010:1–9.
20. Rubie C, Frick VO, Ghadjar P, et al. Effect of preoperative FOLFOX chemotherapy on CCL20/CCR6 expression in colorectal liver metastases. *World J Gastroenterol*. 2011;17:3109–3116.
21. Peters GJ, Backus HHJ, Freemantle S, et al. Induction of thymidylate synthase as a 5-fluorouracil resistance mechanism. *Biochim Biophys Acta*. 2002;1587:194–205.
22. Cassidy J, Taberero J, Twelves C, et al. XELOX (capecitabine plus oxaliplatin): active first-line therapy for patients with metastatic colorectal cancer. *J Clin Oncol*. 2004;22:2084–2091.
23. Lee SJ, Kim SY, Chung JH, et al. Induction of thymidine kinase 1 after 5-fluorouracil as a mechanism for 3'-deoxy-3'-<sup>18</sup>F-fluorothymidine flare. *Biochem Pharmacol*. 2010;80:1528–1536.
24. Li KM, Rivory LP, Hoskins J, Sharma R, Clarke SJ. Altered deoxyuridine and thymidine in plasma following capecitabine treatment in colorectal cancer patients. *Br J Clin Pharmacol*. 2007;63:67–74.
25. Kenny LM, Contractor KB, Stebbing J, et al. Altered tissue 3'-deoxy-3'-<sup>18</sup>F-fluorothymidine pharmacokinetics in human breast cancer following capecitabine treatment detected by positron emission tomography. *Clin Cancer Res*. 2009;15:6649–6657.
26. Hong YS, Kim HO, Kim K, et al. 3'-deoxy-3'-<sup>18</sup>F-fluorothymidine PET for the early prediction of response to leucovorin, 5-fluorouracil, and oxaliplatin therapy in patients with metastatic colorectal cancer. *J Nucl Med*. 2013;54:1209–1216.
27. Yau K, Price P, Pillai RG, Aboagye E. Elevation of radiolabelled thymidine uptake in RIF-1 fibrosarcoma and HT29 colon adenocarcinoma cells after treatment with thymidylate synthase inhibitors. *Eur J Nucl Med Mol Imaging*. 2006;33:981–987.
28. Viertl D, Bischof Delaloye A, Lanz B, et al. Increase of <sup>18</sup>F-FLT tumor uptake in vivo mediated by FdUrd: toward improving cell proliferation positron emission tomography. *Mol Imaging Biol*. 2011;13:321–331.
29. Schelhaas S, Held A, Wachsmuth L, et al. Gemcitabine mechanism of action confounds early assessment of treatment response by 3'-deoxy-3'-<sup>18</sup>F-fluorothymidine in preclinical models of lung cancer. *Cancer Res*. 2016;76:7096–7105.
30. Chiu S-J, Lee Y-J, Hsu T-S, Chen W-S. Oxaliplatin-induced gamma-H2AX activation via both p53-dependent and -independent pathways but is not associated with cell cycle arrest in human colorectal cancer cells. *Chem Biol Interact*. 2009;182:173–182.
31. Saggarr JK, Fung AS, Patel KJ, Tannock IF. Use of molecular biomarkers to quantify the spatial distribution of effects of anticancer drugs in solid tumors. *Mol Cancer Ther*. 2013;12:542–552.
32. Ikeda M, Kurose A, Takatori E, et al. DNA damage detected with γH2AX in endometrioid adenocarcinoma cell lines. *Int J Oncol*. 2010;36:1081–1088.
33. Löbrich M, Shibata A, Beucher A, et al. γH2AX foci analysis for monitoring DNA double-strand break repair: strengths, limitations and optimization. *Cell Cycle*. 2010;9:662–669.